Mapping plasmons in nanoantennas via cathodoluminescence



2008 New J. Phys. 10 105009

(http://iopscience.iop.org/1367-2630/10/10/105009)

New Journal of Physics
The open-access journal for physics

# Mapping plasmons in nanoantennas via cathodoluminescence

**R Gómez-Medina[1,2], N Yamamoto[3], M Nakano[3] and F J García de Abajo[1,4,5]**

[1] Donostia International Physics Center, Aptdo. 1072, 20080 San Sebastian, Spain
[2] Instituto de Ciencia de Materiales de Madrid—CSIC, Sor Juana Inés de la Cruz 3, 28049 Madrid, Spain
[3] Physics Department, Tokyo Institute of Technology, Meguro-ku, Tokyo 152-8551, Japan
[4] Instituto de Óptica—CSIC, Serrano 121, 28006 Madrid, Spain
E-mail: jga@cfmac.csic.es

*New Journal of Physics* **10** (2008) 105009 (13pp)
Received 24 June 2008
Published 28 October 2008
Online at http://www.njp.org/
doi:10.1088/1367-2630/10/10/105009

**Abstract.** We analyze cathodoluminescence (CL) emission from silver nanorod antennas induced by energetic electron beams. The dependence of the emission spectra on particle morphology and electron energy is explored by means of full electromagnetic calculations based on the boundary element method (BEM). We present light-emission image maps obtained by using a light detection system that is incorporated into a transmission electron microscope (TEM), operated in scanning mode. The intensity of each pixel in these maps corresponds to the photon counting rate when the electron beam is focused at that position of the sample. The maps exhibit strong dependence on the polarization of the emitted light and reveal standing-wave patterns of surface plasmons sustained by the nanorods, leading to characteristic spatial variations that correspond to the actual plasmon-mode symmetries. We thus demonstrate direct mapping of plasmon-mode symmetries by observing the variation of the CL intensity as the electron beam scans the sample. Good agreement between experimental and theoretical results is obtained, including the spatial modulation of the intensity along the direction perpendicular to the rods. In particular, plasmon modes of different azimuthal nature are resolved via their characteristic spatial dependence in our polarization-sensitive light detection system.

[5] Author to whom any correspondence should be addressed.

## Contents



## 1. Introduction

The study of metallic nanostructures has received considerable attention in recent years [1]–[3], stimulated in part by the search for new optical materials, to which metals contribute with strong electromagnetic field localization and large electric field enhancement, in contrast to the milder response of dielectrics and semiconductors. In particular, nanoparticles made of noble metals like copper, silver and gold exhibit strong UV-visible extinction bands that have stimulated a broad range of applications in biosensing [4, 5] and signal processing [6]. Light absorption in metallic nanoparticles is intensified by the collective oscillations of conduction electrons known as surface plasmons. The local field under resonant plasmon excitation produces a strong enhancement of the light intensity in the vicinity of the metal, particularly near edges and also in gaps between metallic parts [7]. These properties are of great interest for a number of optical applications such as surface-enhanced Raman scattering (SERS) [8] and plasmonic wave guiding [6, 9, 10].

The frequency of localized surface plasmons depends on the size, shape and composition of the particles on which they are residing and the dielectric environment (substrate and/or solvent) [11, 12]. For instance, the electrostatic dipole resonance in a small metallic sphere requires a metal permittivity $\epsilon = -2$ ($\lambda_{Ag} \simeq 355$ nm, $\lambda_{Au} \simeq 490$ nm), whereas the lowest-order mode in a thin nanowire occurs for $\epsilon = -1$ ($\lambda_{Ag} \simeq 337$ nm, $\lambda_{Au} \simeq 390$ nm). In metallic nanorod antennas, two distinct plasmon resonances are observed, corresponding to induced charge oscillations either parallel (longitudinal) or perpendicular (transverse) to the rod axis. Among these, low-order longitudinal excitations have become increasingly popular for their use as nanoantennas [13, 14].

The study of the near field associated with particle plasmons has been, however, limited by the low resolution available in common techniques such as scanning near-field optical microscopy (SNOM), which can hardly reach below 50 nm. In a separate development, and in contrast to purely optical techniques, local information on plasmons has been obtained for a long time with truly nanometre resolution by relying on fast electrons focused on sub-nanometre spots at a position of the sample. In particular, electron energy loss spectroscopy (EELS) has been used to study plasmons in metallic spheres [15]–[17] and in carbon structures [18], and more recently, to obtain snap shots of plasmons in silver [19] and gold [20] nanoparticles. The maxima in the energy loss spectra of transmitted electrons reflect the energies of the particle–plasmon excitations to which they couple. (Incidentally, electrons can excite plasmons

even if the trajectory does not directly intersect the particle [19].) Part of these energy losses results in the emission of light (cathodoluminescence (CL)), which has also been used to probe localized plasmons in metallic nanoparticles [21]–[23]. Extended surface-plasmon polaritons (SPPs) have also been the subject of pioneering studies using EELS [24] and CL [25]. More recently, fast electrons have been employed to generate SPPs in planar surfaces, the excitation of which has been monitored via the CL emission observed after subsequent outcoupling of the plasmons by a grating [26]–[28]. Plasmons in metallic nanorods [29], metallic ridges [30] and annular plasmonic resonators [31] have been investigated using CL as well.

Here we provide a solid theoretical analysis of CL in metallic nanorods and show that plasmon standing waves lead to oscillations in the electron-induced radiation emission signal as a function of the electron-spot position for wavelengths matching those of the plasmon modes. We supplement our study with experimental results, in qualitative agreement with our calculations. Furthermore, we analyze the light-scattering properties of these particles and compare them with the observed CL. Our work demonstrates that the combination of the high spatial resolution of a TEM, which can focus an electron beam on a $<1$ nm spot at the position of the sample, and the high-energy resolution of a light detection system, below 1 meV in the optical region, can yield relevant information on optical modes with spatial and energy resolution far superior to what is currently available in optical-based techniques such as SNOM. We concentrate on the contribution to light emission originating in the plasmon-assisted CL mechanism induced by the passage of fast electrons through or near a metallic material. Transition radiation [32], produced by the sudden change in the screening of the electron when it crosses a dielectric boundary (e.g. between metal and vacuum), is automatically included in our full solution of Maxwell's equations for the nanorods. We neglect bremsstrahlung radiation [33], which contributes to a featureless background and is very weak for the electron kinetic energies under consideration (100–200 keV). We report polarization-dependent spectrally and spatially resolved measurements and corresponding calculations that provide strong selectivity of spatial patterns for plasmon excitations in metallic particles. The dependence of the spectral features on wavelength and electron-spot position is analyzed for different polarizations, as well as nanorod size and morphology. Our theoretical results are compared with experimental data for one particular geometry. We also discuss the dependence of the emission on the electron velocity. Gaussian atomic units (i.e. $e = \hbar = m = 1$) are used throughout this work unless otherwise specified.

## 2. Theoretical description

We consider isolated submicron silver particles and study the emission of light produced by interaction with a fast external electron. The emission is enhanced when particle plasmons are excited. We assume that the observed particles (figure 1) have a nearly cylindrical shape, so that they can be described as cylindrical rods characterized by their diameter $2d$, the length of its cylindrical section $2L$ and the length of its rounded ends $2d_z$.

Analytical solutions of plasmon modes exist only in simple geometries, such as the sphere or the infinite cylinder. For nanorods, the Maxwell equations need to be solved numerically. Here, we use the boundary element method (BEM) [34, 35], in which the electromagnetic field is expressed in terms of charges and currents distributed on the surface of the particles. In brief, the boundary conditions for the electromagnetic field provide a set of linear integral equations, with charges and currents as unknowns, which are solved self-consistently in the presence of

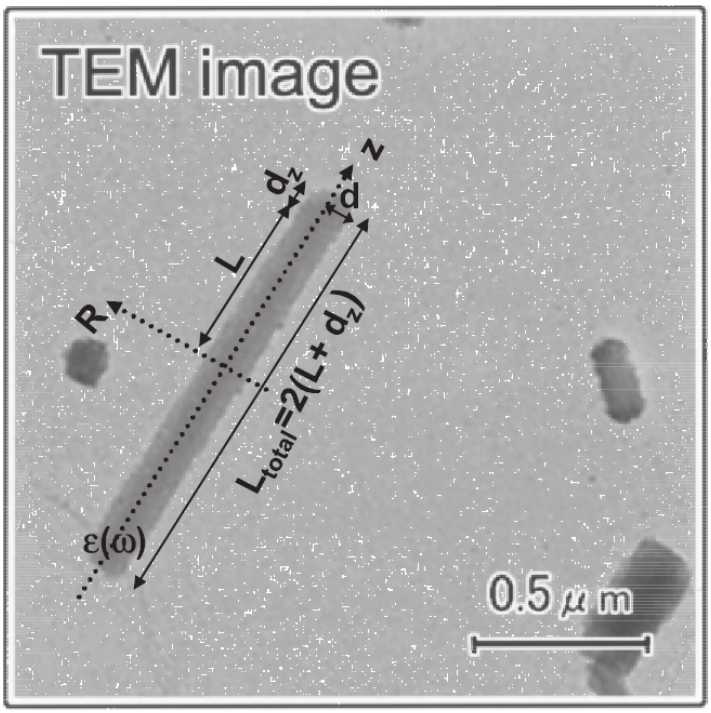


**Figure 1.** Silver nanorod under study. TEM image of a template-grown Ag nanorod, along with some elements of the notation used throughout this work.

the external incident field by discretizing the integrals. The only assumption in this method is that the different media involved in the structures under study are described by frequency-dependent local dielectric functions $\epsilon(\omega)$ and terminate in abrupt interfaces. Our neglect of spatial dispersion is a good approximation for the size of the particles under consideration. We solve Maxwell's equations rigorously using the BEM for an incident field corresponding to either a plane wave (figure 2) or a fast electron (figures 3 and 4). The complex, frequency-dependent dielectric function of silver is taken from optical data [36].

In the BEM [34, 35], the electric and magnetic fields in a nonmagnetic inhomogeneous material are expressed in terms of scalar and vector potentials $\phi$ and $\mathbf{A}$ as $\mathbf{E} = ik\mathbf{A} - \nabla\phi$ and $\mathbf{H} = \nabla \times \mathbf{A}$, respectively, where $k = \omega/c$ is the free-space light momentum. The general solution of the Maxwell equations that vanishes at infinity is then expressed in terms of charges $\sigma_j$ and currents $\mathbf{h}_j$, for $\mathbf{r}$ inside each medium $j$, as

$$\phi(\mathbf{r}) = \phi^{\mathrm{e}}(\mathbf{r}) + \int_{S_j} \mathrm{d}\mathbf{s}\, G_j(|\mathbf{r}-\mathbf{s}|)\sigma_j(\mathbf{s}), \tag{1}$$

$$\mathbf{A}(\mathbf{r}) = \mathbf{A}^{\mathrm{e}}(\mathbf{r}) + \int_{S_j} \mathrm{d}\mathbf{s}\, G_j(|\mathbf{r}-\mathbf{s}|)\mathbf{h}_j(\mathbf{s}), \tag{2}$$

where $S_j$ refers to the boundary of that medium;

$$G_j(|\mathbf{r}-\mathbf{s}|) = \frac{\mathrm{e}^{\mathrm{i}k_j|\mathbf{r}-\mathbf{s}|}}{|\mathbf{r}-\mathbf{s}|} \tag{3}$$

is the scalar Green function; $k_j = k\sqrt{\epsilon_j}$ is the momentum of light inside medium $j$ of permittivity $\epsilon_j$; and $\phi^{\mathrm{e}}$ and $\mathbf{A}^{\mathrm{e}}$ are the scalar and vector potentials that would be created

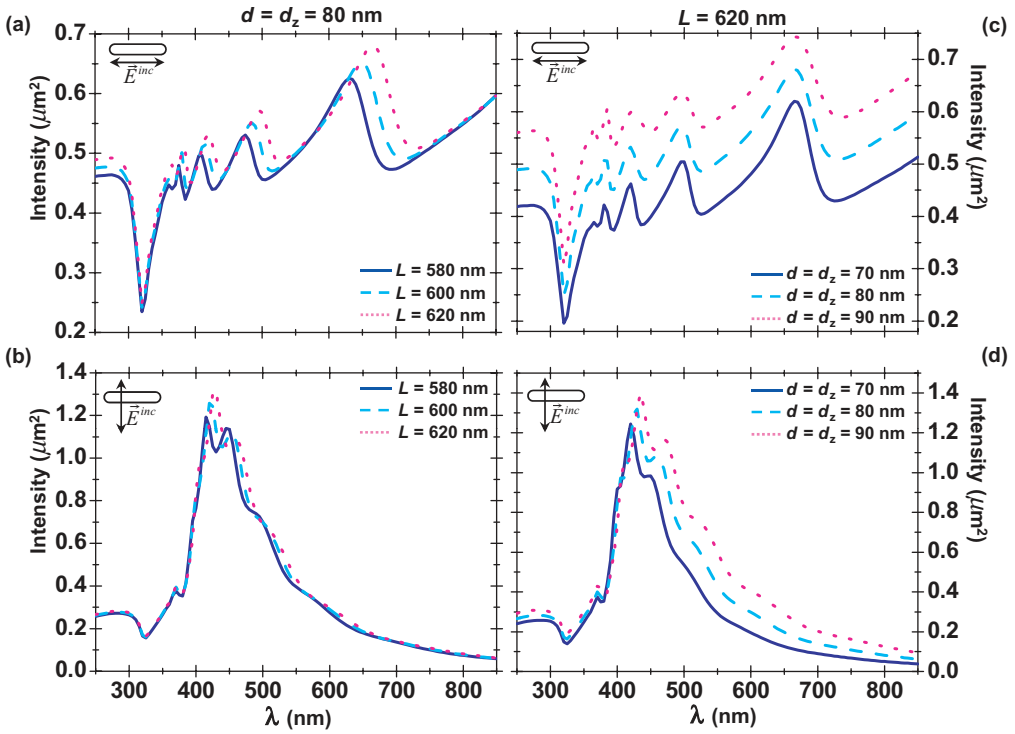


**Figure 2.** Light scattering by silver nanorods. The scattering cross section is plotted as a function of wavelength for an electromagnetic field incident on cylindrical silver nanorods with $d = d_z = 80\,\text{nm}$ and several cylindrical section half-lengths in (a) and (b) and for $L = 620\,\text{nm}$ and different values of the diameter and total length in (c) and (d). The polarization is parallel to the rod axis in (a) and (c) and perpendicular to the rod axis in (b) and (d).

by external charges and currents if only an infinite homogeneous medium $j$ were present. In our case, $j = 1, 2$ labels vacuum and silver, respectively. The boundary conditions of the electromagnetic field are then used to obtain the noted surface integral equations [34, 35]. Furthermore, the axial symmetry of our sample allows parametrizing the nanorod boundary by means of the azimuthal angle with respect to the axial direction, which separates the problem into uncoupled sets of equations, one set for each azimuthal number $m$. Each $m$ component is solved separately, thus minimizing the numerical effort, and effectively reducing the size of the problem to one dimension (the remaining spatial parametrization along the axis of the rod).

Here, we are interested in radiation, either scattered from incoming light or produced by fast electrons. The induced far field can be obtained from the integrals in equations (1) and (2) in the $kr \to \infty$ limit (the radiation is produced and measured outside the rod, where $k_1 = k$), for which $G_1 \approx \exp[\mathrm{i}(kr - k\hat{\mathbf{r}}\cdot\mathbf{s})]/r$, where $\hat{\mathbf{r}} = \mathbf{r}/r$. Then, the induced far field reduces to

$$\mathbf{E}^{\text{ind}}(\mathbf{r}) = \frac{\mathrm{e}^{\mathrm{i}kr}}{r}\mathbf{f}(\Omega), \tag{4}$$

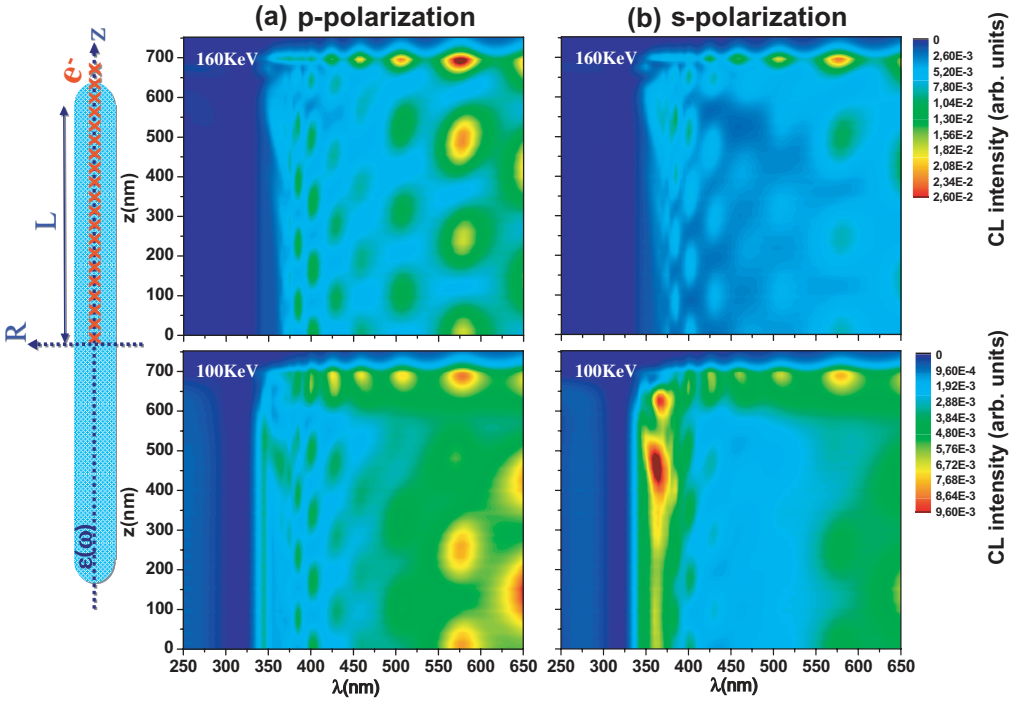


**Figure 3.** Dependence of CL emission on photon wavelength and electron energy. The contour plots show CL intensities from a silver nanorod with $L = 620$ nm and $d = d_z = 80$ nm in a space–wavelength map ($z$–$\lambda$) taken at two different electron energies (see text insets) when the position of the electron beam probe is located along the rod axis at a distance $z$ from its center (see sketch on the left). The polarization of emitted light is parallel to the rod axis in (a) and perpendicular to the nanorod axis in (b).

where $\Omega$ denotes the orientation of $\mathbf{r}$ and the far-field amplitude $\mathbf{f} = \mathbf{g} - (\mathbf{g}\cdot\hat{\mathbf{r}})\hat{\mathbf{r}}$ is expressed in terms of the boundary current on the vacuum side as

$$\mathbf{g}(\Omega) = \mathrm{i}k \int_{S_1} \mathrm{d}\mathbf{s}\, \mathrm{e}^{-\mathrm{i}\hat{\mathbf{r}}\cdot\mathbf{s}} \mathbf{h}_1(\mathbf{s}). \tag{5}$$

Notice that we have used the fact that the contribution of $-\nabla\phi$ to $\mathbf{E}$ gives rise to longitudinal components of the field. However, the far field has to be radiation-like, that is, transversal, and thus entirely coming from the $\mathrm{i}k\mathbf{A}$ contribution to $\mathbf{E}$, which gives rise to $\mathbf{g}$ (equation (5)), from which the longitudinal part has been subtracted in order to find the far-field amplitude $\mathbf{f}$.

The far-field amplitude is directly related to the angle-resolved scattering cross section via [37]

$$\frac{\mathrm{d}\sigma}{\mathrm{d}\Omega} = |\mathbf{f}(\mathbf{\Omega})|^2 \tag{6}$$

for incident radiation. Similarly, the CL intensity can be obtained from the Poynting vector integrated over emission directions. The emitted energy per incoming electron is then given by

$$\Delta E = \frac{c}{4\pi} \int \mathrm{d}t\, r^2 \int \mathrm{d}\Omega\ \hat{\mathbf{r}} \cdot [\mathbf{E}(\mathbf{r}, t) \times \mathbf{H}(\mathbf{r}, t)]. \tag{7}$$

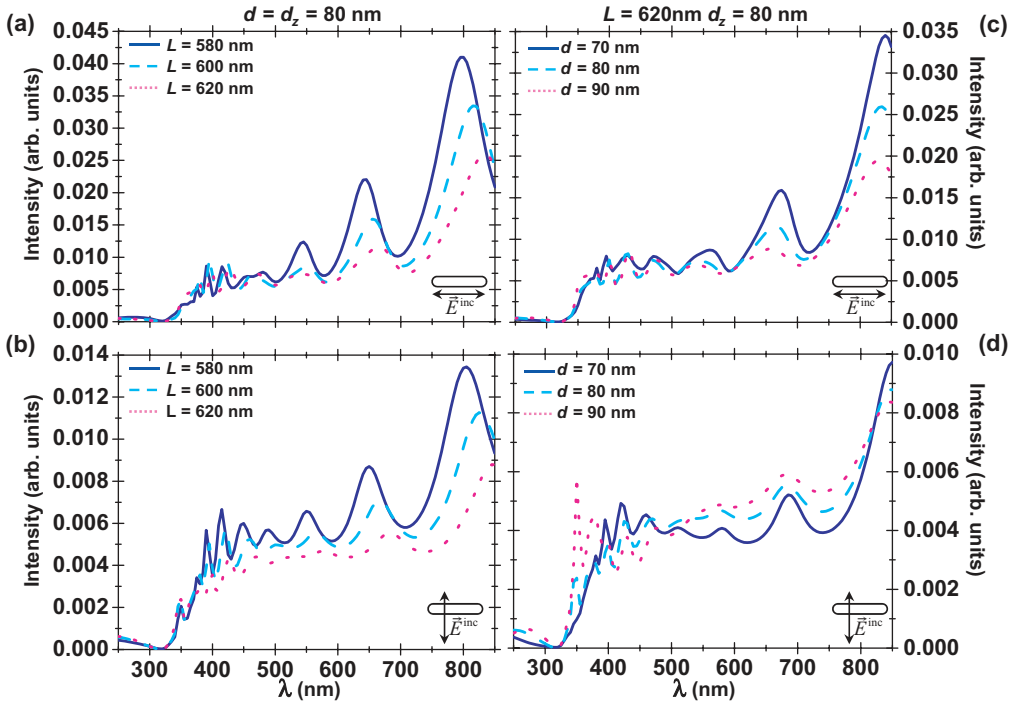


**Figure 4.** Dependence of CL photon emission on nanorod geometry. CL emission spectra from silver rods are shown in (a) and (b) for $d = d_z = 80\,\text{nm}$ and several values of $L$, and in (c) and (d) for $L = 620\,\text{nm}$, $d_z = 80\,\text{nm}$, and different diameters. The spectra have been calculated for an electron energy of 160 keV and with the electron beam focused near the nanorod edge. The polarization is parallel to the rod axis in (a) and (c), and perpendicular to the rod axis in (b) and (d).

Now, expressing the fields in time Fourier transform and using the far-field limit just discussed, $\Delta E$ can be decomposed into photon-energy components $\omega$ as

$$\Delta E = \int_0^\infty \omega \, \mathrm{d}\omega \int \mathrm{d}\Omega \; P(\Omega, \omega), \tag{8}$$

where

$$P(\Omega, \omega) = \frac{1}{4\pi^2 k} |\mathbf{f}(\Omega)|^2 \tag{9}$$

is the number of photons emitted per incoming electron per unit time per unit of solid angle of emission $\Omega$ and per unit of photon energy range $\omega$. In what follows, we integrate equations (6) and (9) over scattering/emission angles to obtain light scattering cross sections and CL intensities.

## 3. Light scattering

Let us first discuss the response of a cylindrical rod when it is illuminated by a plane wave incident perpendicular to the nanorod and with the light polarized either parallel or

perpendicular to the nanorod axis. This can help us understand CL photon emission induced by high-energy electrons. In particular, this will unveil the excitation wavelengths characteristic of the particle for which the process of emission induced by passing electrons is enhanced.

Figure 2 shows the dependence of the far-field intensity on incident wavelength $\lambda$ for cylindrical silver nanorods with hemispherical rounded caps (i.e. $d = d_z$). As shown in figures 2(a) and (c), the spectral peaks shift to longer wavelengths with increasing $L$ for parallel polarization, while no strong dependence on $d$ or $d_z$ is observed. This can be understood in a standing-wave picture, so that the longer the rod, the larger the wavelength of the surface oscillations, and therefore, the larger the photon wavelength to which they couple. For parallel polarization, only even modes $m$ can be excited, and the mode $m = 0$ is actually dominant for the diameter of the particle under consideration. In this mode, the induced charges and currents vary only along the particle length, which explains why $L$ is the most relevant parameter in this case, as already observed in experimental measurements of colloidal nanorods [38]. Furthermore, the peak intensities are enhanced when both $L$ and $d$ increase, since the actual strength of the coupling to external light increases with particle size. At the same time, the features become broader, owing to the contribution originating in the coupling of the plasmon mode with radiation (radiation leakage), which increases with particle size.

When the incident light is polarized perpendicular to the rod axis (figures 2(b) and (d)), the spectral features become more intense and shift to longer wavelengths with increasing $d$, while the peak positions are only slightly affected by $L$. In this case, only odd azimuthal modes $m$ can be excited, and $m = \pm 1$ is the dominant one. The major source of self-interaction between charges and currents induced on the particle comes from regions on opposite sides within its transversal cross section, so that the particle radius $d$ is the most relevant parameter. The length of the particle also has an influence, but sign cancellations between contributions from different regions along the axis of the particle effectively reduce the dependence on $L$.

## 4. Emission spectra

The CL emission induced by an energetic electron beam passing through or near a silver nanorod is studied separately for each polarization direction of the emitted light, either parallel (p) or perpendicular (s) to the rod axis. Although silver particles are supported by a carbon film in the experimental setup that we report later on, we neglect the substrate in the calculations that follow and therefore consider that the nanorods are self-standing in vacuum, thus making our results more general.

Figure 3 shows calculated contour plots of emission spectra from a silver nanorod obtained for different electron energies when the position of the electron beam spot is scanned along the rod axis (see the sketch in figure 3). Overall, we obtain oscillation patterns similar to those observed recently using smaller electron acceleration voltages [29]. Clearly, the position of emission features and the number of them are independent of the electron velocity. Moreover, with independence of the polarization of the emitted light, we observe that the peak intensities are enhanced when the electron energy is increased, except for the region close to $\lambda \approx 365$ nm, where the sharp peaks observed at 100 keV and originating in bulk plasmon excitation are very much reduced at 160 keV. Furthermore, these contour plots reveal node–antinode patterns inside the rod, consistent with a standing-wave picture. Notice in particular that the number of peaks decreases when the wavelength becomes larger. This can be understood from the above discussion of light scattering (section 3).

We concluded in section 3 that the half-length of the cylindrical section $L$ and the radius of the rod $d$ are the most important parameters that determine the positions and intensities of spectral features. In agreement with this observation, the emission spectra presented in figure 4 for an electron beam focused close to one of the nanorod ends show that the spectral peaks are red-shifted when $L$ increases (figures 4(a) and (c)) but are hardly affected by variations in $d$ or $d_z$. Furthermore, when $L$ or $d$ increases, the long-wavelength peaks become weaker, in sharp contrast with the results obtained for light scattering. This different behavior can be understood from the localized character of the electron probe: longer-wavelength modes have smaller intensity at the position of the beam, outside the particle; this is in contrast with light scattering, in which the coupling involves the entire extension of the particle.

## 5. CL photon maps

Figure 5 presents experimental and theoretical photon maps of a silver nanorod taken at (a) $\lambda = 360$ nm, (b) $\lambda = 460$ nm and (c) $\lambda = 600$ nm for the p-polarized emitted light and (d) $\lambda = 580$ nm for the s-polarized component. The electron energy is 160 keV in all cases. These maps have been obtained by scanning the electron beam over the sample region in a scanning mode of operation and by simultaneously detecting photons at selected wavelengths. The intensity of each pixel represents the photon rate measured when the electron beam is positioned at that spot of the sample. This imaging technique is similar to SEM mapping, except that we use the light intensity collected by the ellipsoidal mirror rather than secondary electrons. A similar analysis has recently been reported [29], which we supplement here by discussing the polarization dependence of the CL signal.

Silver nanorods were produced by evaporation in an Ar atmosphere and collected in a TEM sample holder. Emission rates were acquired by a light detection system combined with a standard TEM (JEM-2000FX). The light emitted from individual nanorods was collected by an ellipsoidal mirror (acceptance angles 3.6–84°) and focused on the entrance slit of a monochromator outside the TEM. A linear polarizer was placed between the mirror and the monochromator to select linearly polarized components of the emitted light. This system permits spectrally and spatially resolved measurement of p- and s-polarization components independently, as described elsewhere [21]–[23]. A GaAs photomultiplier tube was used for light in the 250–850 nm optical region. The diameter of the electron beam spot at the position of the target was 10 nm. This is a relatively large value that was used in order to allow for higher beam currents ($\sim$1 nA), and therefore, a sufficiently high photon count rate. However, the beam diameter is still much smaller than both the size of the nanorod ($\sim 1\ \mu$m) and the typical length scales involved in the extension of the surface modes along the particle surface.

The parameters of the nanorod in our calculated photon maps have been chosen in such a way that the wavelength and the number of bright spots along the particle are the same for the modes represented in the experiment. This has resulted in a best-fit half-length of $L = 330$ nm, much smaller than the half-length of $L = 620$ nm obtained from the TEM image of figure 1. This difference in length can be attributed to the approximations that have been made to describe the particle: (i) the section is assumed to be circular, and the effect of crystallographic facets has been ignored; (ii) the simulated particle is self-standing, whereas the experiment relies on particles sitting on the carbon substrate of a TEM sample holder, possibly leading to large shifts in the spectral features; (iii) the simulated particles are considered to be made of pure bulk silver, whereas the actual particles can have porosity and chemical contamination, leading to

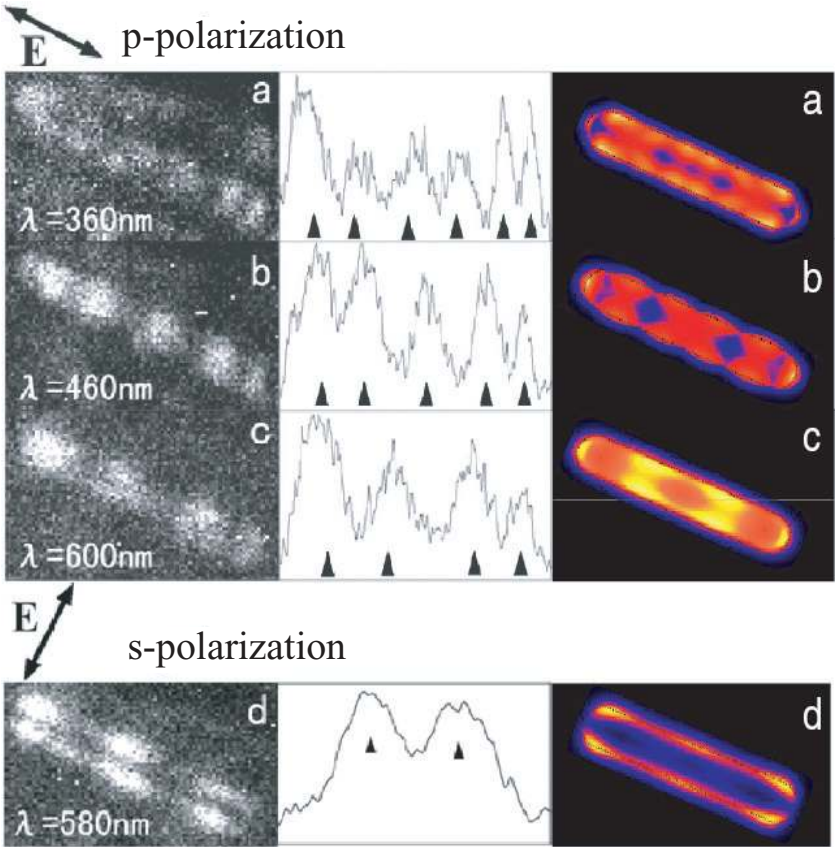


**Figure 5.** Comparison of measured and calculated photon emission intensity maps for different light polarizations. Here we show experimental (left part) and theoretical (right part) CL photon maps of silver rods with $L = 620$ nm and $L = 330$ nm, respectively, for an electron energy of 160 keV. The polarization of emitted light is parallel to the rod axis in (a), (b) and (c) and perpendicular to the rod axis in (d). Each pixel in the experimental image corresponds to a different position of the electron beam, and the intensity of the pixel is made proportional to the emission rate of the selected light polarization component. Dark (bright) regions in these single-wavelength maps correspond to low (high) photon emission intensity. The central part of the figure shows measured emission rates along the rod axis (a)–(c) and along its edge (d).

modified dielectric response. All of these effects are effectively wrapped up in our choice of a fitted length of the particle, leading to otherwise excellent agreement between theoretical and experimental photon maps when they are scaled by the nanorod length.

Figure 5 exhibits oscillations in the image contrast along the nanorod axis, which can be ascribed again to standing waves produced by interference of surface plasmons propagating along the rod and reflected at its ends, leading to a Fabry–Perot condition for the wavelengths at which the modes exist. Strong emission can be expected to occur when the incident electron beam illuminates an antinode position of the standing wave, where surface plasmon excitation should be most efficient. The rod acts like an antenna and significant radiative decay of the excited plasmon takes place, which contributes to CL. From the observed photon maps one

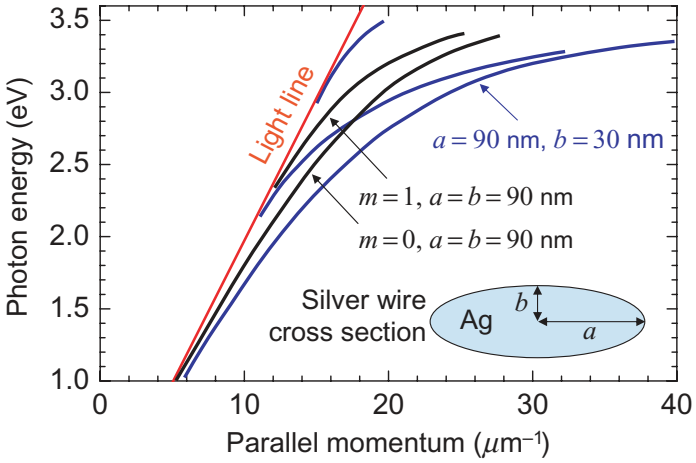


**Figure 6.** Plasmon dispersion relation in infinitely long silver wires of circular and elliptical cross section. The plasmon energy is shown as a function of momentum parallel to the axis of the wires. The azimuthal number $m$ is relevant in circular wires ($m = 0$ and $m = 1$ modes are considered here). The three lowest-energy modes of an elliptical wire are also shown in the figure.

can conclude that the rod caps act as antinodes. Since a standing wave corresponding to an $n$th-order mode has $n$ nodes along the rod, the maps offered in figure 5 can be assigned the values (a) $n = 5$, (b) $n = 4$, (c) $n = 3$ and (d) $n = 2$, respectively. In agreement with the theoretical photon maps (figure 3(b)), the number of peaks decreases from 6 to 4 with increasing wavelength from (a) to (c).

It should be mentioned that the bright spots corresponding to p-polarized emitted light (figures 5(a)–(c)) are centered along the axis of the rod, and this is consistent with the dominant role played by the $m = 0$ plasmon, as mentioned above. However, the s-polarized emission (figure 5(d)) has brighter contrast along the two side edges of the nanorod, also consistent with a dominant $m = \pm 1$ contribution.

The noted standing-wave picture can be elaborated from the dispersion relation of infinite wires by looking at values of the momentum parallel to the wire axis equal to multiples of one quantum of rod-cavity momentum $\pi/2L_{\text{eff}}$ (i.e. this quantity multiplied by the number of antinodes), where $L_{\text{eff}}$ is an effective nanorod half-length, corrected for the effect of the caps [13]. Figure 6 shows the dispersion of plasmons of $m = 0$ and $m = 1$ azimuthal symmetry in infinitely long circular wires of diameter similar to the rods considered throughout this work. The $m = 1$ plasmon frequency lies above the $m = 0$ mode, which explains why the two-node mode resolved with s-polarization can have higher energy (i.e. shorter wavelength) than the three-node mode resolved with p polarization in figure 5. Furthermore, the lowest-frequency plasmon ($m = 0$ in circular rods) shifts to the red when the wire is compressed in one direction to become an elliptical wire (see figure 6), while the second-lowest mode ($m = 1$ in circular rods) is split into two modes (one of them pushed very close to the light line). This dramatic change in mode frequency illustrates how severely the nanorod cross section affects the plasmon energies, thus illustrating the need for simultaneously assessing the particle geometry and its optical response.

## 6. Conclusions

We have analyzed CL photon emission from silver nanorod antennas both theoretically and experimentally and compared the results with light scattering properties of these particles. The role of various parameters characterizing the rod geometry has been addressed. Furthermore, the dependence of the CL signal on electron energy has been examined, and we have concluded that the wavelength of the emission features and the number of such features in the spectra are independent of electron energy, while the relative intensities of the observed peaks change with electron velocity. With independence of the polarization of the emitted light, the spectral features are enhanced when the electron energy is increased, except for wavelengths around 365 nm (near the bulk plasmon of silver), for which the opposite behavior is observed: higher velocities imply larger extension of the evanescent field accompanying the electron (for a frequency $\omega$, the field decays exponentially away from the trajectory, reaching a distance $\sim v/\omega$), and thus, also larger coupling to the standing plasmon waves of the rods; in contrast, an increase of velocity results in weaker coupling to bulk plasmons, which vary more rapidly in space than surface plasmons.

We have also found that emission spectra and photon maps obtained by scanning the electron beam over the sample exhibit remarkable differences in spatial distribution depending on the polarization direction of the emitted light. The p-polarized component of the emission (i.e. with the polarization of the emitted light parallel to the rod axis) shows intensity maxima when the beam intersects the rod axis, while the s-polarized component (polarization perpendicular to the axis) finds its maxima along the two side edges of the rod. We attribute these results to the excitation of rod plasmons with different azimuthal dependences: the p- and s-polarized emissions are dominated by $m = 0$ and $m = \pm 1$ plasmons, respectively.

## Acknowledgments

We thank N I Zheludev, M Kociak and A Polman for stimulating discussions. This work has been supported in part by the Spanish MEC (contracts NAN2004-08843-C05-05 and MAT2007-66050) and by the EU-FP6 (NMP4-2006-016881 'SPANS').

## References

[1] Kreibig U and Vollmer M 1995 *Optical Properties of Metal Clusters* (Berlin: Springer)
[2] Burda C, Chen X, Narayanan R and El-Sayed M A 2005 *Chem. Rev.* **105** 1025–102
[3] Zia R, Schuller J A, Chandran A and Brongersma M L 2006 *Mater. Today* **9** 20–7
[4] Nie S and Emory S R 1997 *Science* **275** 1102–6
[5] Talley C E, Jackson J B, Oubre C, Grady N K, Hollars C W, Lane S M, Huser T R, Nordlander P and Halas N J 2005 *Nano Lett.* **5** 1569–74
[6] Krenn J R *et al* 1999 *Phys. Rev. Lett.* **82** 2590–3
[7] Danckwerts M and Novotny L 2007 *Phys. Rev. Lett.* **98** 026104
[8] Xu H, Bjerneld E J, Käll M and Börjesson L 1999 *Phys. Rev. Lett.* **83** 4357–60
[9] Maier S A, Kik P G, Atwater H A, Meltzer S, Harel E, Koel B E and Requicha A A G 2003 *Nat. Mater.* **2** 229–32
[10] Sweatlock L A, Maier S A, Atwater H A, Penninkhof J J and Polman A 2005 *Phys. Rev.* B **71** 235408
[11] Liz-Marzán L M 2006 *Langmuir* **22** 32–41

[12] Myroshnychenko V, Rodríguez-Fernández J, Pastoriza-Santos I, Funston A M, Novo C, Mulvaney P, Liz-Marzán L M and García de Abajo F J 2008 *Chem. Soc. Rev.* **37** 1792–1805
[13] Novotny L 2007 *Phys. Rev. Lett.* **98** 266802
[14] Bryant G W, García de Abajo F J and Aizpurua J 2008 *Nano Lett.* **8** 631–6
[15] Cowley J M 1982 *Phys. Rev.* B **25** 1401–4
[16] Batson P E 1985 *Surf. Sci.* **156** 720–34
[17] Ugarte D, Colliex C and Trebbia P 1992 *Phys. Rev.* B **45** 4332–43
[18] Kociak M, Henrard L, Stéphan O, Suenaga K and Colliex C 2000 *Phys. Rev.* B **61** 13936–44
[19] Nelayah J *et al* 2007 *Nat. Phys.* **3** 348–53
[20] Bosman M, Keast V J, Watanabe M, Maaroof A I and Cortie M B 2007 *Nanotechnology* **18** 165505
[21] Yamamoto N, Araya K, Toda A and Sugiyama H 2001 *Surf. Interface Anal.* **31** 79–86
[22] Yamamoto N, Araya K and García de Abajo F J 2001 *Phys. Rev.* B **64** 205419
[23] Yamamoto N, Nakano M and Suzuki T 2006 *Surf. Interface Anal.* **38** 1725–30
[24] Vincent R and Silcox J 1973 *Phys. Rev. Lett.* **31** 1487–90
[25] Heitmann D 1977 *J. Phys. C: Solid State Phys.* **10** 397–405
[26] Bashevoy M V, Jonsson F, Krasavin A V, Zheludev N I, Chen Y and Stockman M I 2006 *Nano Lett.* **6** 1113–5
[27] van Wijngaarden J T, Verhagen E, Polman A, Ross C E, Lezec H J and Atwater H A 2006 *Appl. Phys. Lett.* **88** 221111
[28] Bashevoy M V, Jonsson F, MacDonald K F, Chen Y and Zheludev N I 2007 *Opt. Express* **15** 11313
[29] Vesseur E J R, de Waele R, Kuttge M and Polman A 2007 *Nano Lett.* **7** 2843–6
[30] Vesseur E J R, de Waele R, Lezec H J, Atwater H A, García de Abajo F J and Polman A 2008 *Appl. Phys. Lett.* **92** 083110
[31] Hofmann C E, Vesseur E J R, Sweatlock L A, Lezec H J, García de Abajo F J, Polman A and Atwater H A 2007 *Nano Lett.* **7** 3612–7
[32] Ginzburg V L and Frank I M 1946 *Zh. Eksp. Teor. Fiz.* **16** 15–28
Ginzburg V L and Frank I M 1946 *Sov. Phys.—JETP* **16** 15–28 (Engl. Transl.)
[33] Jackson J D 1999 *Classical Electrodynamics* (New York: Wiley)
[34] García de Abajo F J and Howie A 1998 *Phys. Rev. Lett.* **80** 5180–3
[35] García de Abajo F J and Howie A 2002 *Phys. Rev.* B **65** 115418
[36] Johnson P B and Christy R W 1972 *Phys. Rev.* B **6** 4370–9
[37] Bohren C F and Huffman D R 1983 *Absorption and Scattering of Light by Small Particles* (New York: Wiley-Interscience)
[38] Xia Y, Yang P, Sun Y, Wu Y, Mayers B, Gates B, Yin Y, Kim F and Yan H 2003 *Adv. Mater.* **15** 353–89